






The Effect of Material Properties on Oxygen Evolution Activity and Assessing Half-Cell Screening as a Predictive Tool in Electrolysis

Shaun M. Alia,^{1,z}  Judith Manco,² Grace C. Anderson,¹  Katherine E. Hurst,¹  and Christopher B. Capuano²

¹Chemistry and Nanoscience Center, National Renewable Energy Laboratory, Golden, Colorado 80401, United States of America

²NEL Hydrogen, Wallingford, Connecticut 06457, United States of America

Iridium-based oxygen evolution catalysts are screened in this study for activity and stability with rotating disk electrode (RDE) half-cells. This study focuses on the electrochemical and materials approaches needed to characterize oxygen evolution catalysts, and include testing for activity, stability, composition, oxide content, and structure. Findings also discuss recommendations for data interpretation and detail the difficulties of comparing catalysts across materials sets with different elemental and oxide compositions, and linking RDE activity to device-level performance. The materials evaluated are a mixture of oxides and metals, and several methods are used to quantify metal content, qualitatively assess oxide content, and determine total surface area. Oxygen evolution activities and stabilities are compared, where a wide range of results are reported. In general, higher RDE performances are found for catalysts that contained larger amounts of ruthenium and metals. Higher durability, however, is found for catalysts that only contained iridium and a higher proportion of oxides. Additionally, catalysts are evaluated for performance in membrane electrode assemblies to assess RDE as a predictive tool in electrolysis. While activity trends within individual material sets generally held between ex- and in-situ testing, RDE tends to overestimate the activity of more metallic catalysts when compared to device-level performance. These results stress the need for multiple metal/oxide baselines for mixed catalysts, to better project in-situ kinetics.

© 2021 The Author(s). Published on behalf of The Electrochemical Society by IOP Publishing Limited. This is an open access article distributed under the terms of the Creative Commons Attribution Non-Commercial No Derivatives 4.0 License (CC BY-NC-ND, <http://creativecommons.org/licenses/by-nc-nd/4.0/>), which permits non-commercial reuse, distribution, and reproduction in any medium, provided the original work is not changed in any way and is properly cited. For permission for commercial reuse, please email: permissions@iopublishing.org. [DOI: [10.1149/1945-7111/ac28c5](https://doi.org/10.1149/1945-7111/ac28c5)]



Manuscript submitted May 19, 2021; revised manuscript received August 23, 2021. Published October 4, 2021.

Hydrogen today plays a relatively small role in energy pathways, primarily in ammonia production (agriculture) and oil upgrading (transportation). Due to lower production cost, most commercial hydrogen is made through steam methane reforming.¹ The use of low cost, renewable power, however, can improve the cost competitiveness of producing hydrogen through electrochemical water splitting by reducing the feedstock cost.²

Within low temperature, proton exchange membrane-based electrolysis, catalyst development is of interest for performance, cost, and durability considerations. Higher performing catalysts can lessen load requirements, potentially slowing durability losses or allowing for platinum (Pt) group metal (PGM) loading reductions.^{3–7} Catalyst development efforts typically focus on the oxygen evolution reaction (OER) at the anode due to the slow kinetics compared to hydrogen evolution and higher durability concerns at elevated potential.^{8–11} Iridium (Ir)-based materials are often used in acidic OER due to moderate activity and a relatively low dissolution rate.^{10–12} Other elements, however, are often added to improve performance (ruthenium, Ru) or stability, or used in conjunction with supports to improve site access (niobium, Nb).^{13–19} Additionally, different Ir surfaces, structures (morphology), and alloys have been used to improve upon OER activity as well.^{20–30}

In acidic OER, previous efforts have established baselines for ex-situ performance, optimized ex-situ coating processes and characterization techniques, and developed methods for determining catalyst surface areas and site-specific activities.^{8,31–33} Catalyst durability studies have included comparing relative stabilities and exploring accelerated stress tests for operation at constant and intermittent input, including accounting for hydrogen crossover and catalyst redox transitions.^{8,11,12,31,33–36} Studies have also sought to correlate ex- and in-situ performance/durability, and found that while rotating disk electrodes (RDEs) can inform membrane electrode assembly (MEA) performance/durability, catalyst composition and metal/

oxide content can complicate comparisons and limit the effectiveness of RDE as a predictive tool.^{34,37}

In this study, catalysts were tested ex- and in-situ as part of a HydroGEN Energy Materials Network project investigating Ir-based OER catalysts in proton exchange membrane-based electrolyzers.³⁸ This study focuses on the approaches needed to characterize OER catalysts, including electrochemical (activity, stability, surface area) and materials (composition, oxide content, structure) experiments. These findings also provide recommendations for data interpretation and detail the difficulties of comparing catalysts across materials sets with different elemental and oxide compositions, and linking RDE activity to device-level performance.

Experimental

Catalyst composition was determined with inductively coupled plasma-mass spectrometry (ICP-MS) using a Thermo Scientific iCAP Q run in standard and kinetic energy discrimination (KED) modes (Table I). Catalyst samples (1 mg) were ashed with sodium peroxide (in excess of 4 mg) in a zirconium crucible using a Meker-Fisher burner. The ashed samples were dissolved in water, nitric acid, and hydrochloric acid (1:1:1 volumetric), diluted to 2, 20, and 200 ppb, and filtered (0.4 μm). The ICP-MS was calibrated to a blank, internal standards, and Ir/ruthenium (Ru)/niobium (Nb) standards at concentrations of 2, 20, and 200 ppb. For the analysis of these samples, the ICP-MS detection limit (IDL) was less than 4 ppt for the elements evaluated (< 1 ppt Ir, 1 ppt Ru, 3 ppt Nb). Oxide content was approximated by as the intended concentration (2, 20, 200 ppb) less the metal concentration detected. Composition was confirmed with energy dispersive X-ray spectroscopy (EDS), taken during microscopy.

X-ray diffraction (XRD) experiments were completed with a Bruker D8 Discover. Samples were fixed with carbon tape onto a silica slide and XRD patterns were taken at 40 kV and 35 mA over 13.5°–88° 2 θ . Rietveld refinement of the XRD patterns was used to determine an average crystallite size and completed with Match 3.2.2 and FullProf 2.05. Field emission scanning electron

^zE-mail: shaun.alia@nrel.gov

Table I. Catalyst composition determined by ICP-MS and RDE activities (exchange current density, i_0 , and Tafel slope).

Sample	Ir [wt.%]	Ru [wt.%]	Nb [wt.%]	O [wt.%]	i_0 [$\mu\text{A g}^{-1}$]	Tafel Slope [mV dec^{-1}]
1.1 Ir	98.3	–	–	1.7	152	48.9
1.2 IrO ₂	84.8	–	–	15.2	90	49.8
2.1 Ir	86.2	–	–	13.8	156	50.8
2.2 Ir Ru	41.5	45.9	–	12.6	481	50.4
2.3 Ir Ru	37.5	48.7	–	13.8	459	51.1
3.1 Ir	98.7	–	–	1.3	26	48.4
3.2 Ir	94.1	–	–	5.9	31	50.0
4.1 Ir Ru	59.0	30.4	–	10.6	214	46.9
4.2 Ir Ru	54.3	42.1	–	3.6	147	48.9
5.1 Ir	85.6	–	–	14.4	40	47.9
5.2 Ir Ru	84.3	3.2	–	12.5	31	47.2
5.3 Ir	86.9	–	–	13.1	258	52.6
5.4 Ir Ru Nb	69.2	2.9	17.6	10.4	14	46.8

microscopy (SEM) was completed with a Hitachi S-4800 at 15 kV. Samples were dispersed in water and isopropanol, briefly sonicated, and pipetted onto silica slides that were fixed to the sample holder with carbon tape. Brunauer–Emmett–Teller (BET) experiments were completed with a Micromeritics Autosorb 2020 and samples were held at 120 °C (1 h) to desorb water.

Working RDEs were coated using previous established methods.³¹ Catalyst (3.5 mg, metal basis) was added to 7.6 ml of water and 2.4 ml of isopropanol, briefly sonicated, and iced for 5 min. Nafion ionomer (20 μl of 5 wt.%, Sigma Aldrich) was then added to the ink, which was horn sonicated for 30 s, bath sonicated for 20 min, and horn sonicated for 30 s in ice. The ink was pipetted (10 μl) onto machine polished gold polycrystalline electrodes, rotating (face-up) at 100 rpm. After pipetting the ink, the electrode rotation was set to 700 rpm and the electrodes allowed to dry at room temperature (20 min).

RDE testing was completed with coated gold polycrystalline working electrodes, a gold mesh counter, and a reversible hydrogen (RHE) reference in a 0.1 M perchloric acid electrolyte (ACS). Electrochemical measurements were taken with an Autolab PGSTAT302N (Eco Chemie, Metrohm Autolab BV) and working electrode rotation was controlled with a modulated speed rotator (Pine Research Instrumentation). Working electrodes were conditioned by cycling at elevated potential, 50 cycles at 100 mV s^{-1} in the range 1.2–1.8 V vs RHE while rotating at 2500 rpm. OER activities were determined with linear sweep voltammograms at 20 mV s^{-1} in the potential range 1.2–1.65 V to focus on kinetics and 1.2–2.0 V to include the entire potential region of interest while rotating at 2500 rpm. Resistance corrections (24–26 Ω) were determined from a current interrupt at 1.6 V, corrected OER linear sweep voltammograms for ohmic loss, and were a function of distance between the working and reference electrodes and the electrolyte conductivity. Linear sweep voltammograms were corrected for internal resistance in the program file to avoid data processing inaccuracies. For reproducibility, eight electrodes were tested for each catalyst. Standard deviations were included in comparison plots of OER activities and were 5% or less, and likely aided by the electrodes being coated with the same ink at the same time.

OER activities were also taken with successive chronoamperometry experiments, for catalyst baselines and select materials (Fig. 1). Chronoamperometry tests were taken every 25 mV (1.4–1.6 V vs RHE) for a 5 s duration, to minimize transport losses due to longer experiment duration and higher gas generation rates. Throughout this study, OER activities were compared from linear sweep voltammograms in the kinetic region, at a potential greater than capacitive interference and a potential lower than the transport onset. Chronoamperometry tests were not used for comparisons, due to the higher transport losses at moderate current/potential, and since

the higher transport losses disproportionately affect high performing catalysts (higher gas generation rates). Past efforts also evaluated chronoamperometry duration and sampling frequency on baseline catalysts and similarly noted difficulties comparing kinetics at moderate current/potential.³¹

Electrochemical surface areas (ECAs) were evaluated with hydrogen underpotential deposition, carbon monoxide oxidation, and mercury underpotential deposition.³² Cyclic voltammograms in a nitrogen-saturated 0.1 M perchloric acid electrolyte were taken in the potential range 0.025–1.5 V vs RHE at a scan rate of 20 mV s^{-1} . Hydrogen underpotential deposition ECAs were calculated from the charge due to an adsorbed monolayer assuming a charge conversion of 179 $\mu\text{C cm}_{\text{Ir}}^{-2}$ and 125 $\mu\text{C cm}_{\text{Ru}}^{-2}$. Carbon monoxide stripping was conducted in a 0.1 M perchloric acid electrolyte with a 20 min hold at 0.2 V, the first 10 min under a carbon monoxide purge and the second 10 min under a nitrogen purge. After the 20 min hold, 3 cyclic voltammograms were completed (starting anodically) in the range 0.025–1.5 V vs RHE at 20 mV s^{-1} . Carbon monoxide ECAs were calculated from the first scan with the charge due to the oxidation of the adsorbed carbon monoxide monolayer, assuming a charge conversion of 358 $\mu\text{C cm}_{\text{Ir}}^{-2}$ and 250 $\mu\text{C cm}_{\text{Ru}}^{-2}$. Subsequent scans were used to confirm Mercury underpotential was completed in a nitrogen saturated 0.1 M perchloric acid electrolyte containing 1 mM mercury nitrate (Sigma Aldrich). Cyclic voltammograms were completed in the potential range 0.025–0.55 V vs RHE at a scan rate of 20 mV s^{-1} . Mercury underpotential deposition ECAs were calculated from the charge due to an adsorbed mercury monolayer, assuming a charge conversion of 358 $\mu\text{C cm}_{\text{Ir}}^{-2}$ and 301 $\mu\text{C cm}_{\text{Ru}}^{-2}$.^{32,39} Following initial ECA testing, all catalysts were held at 0.2 V vs RHE in a nitrogen saturated 0.1 M perchloric acid electrolyte for 13.5 h to ensure near-surface reduction and retested with mercury underpotential deposition.³⁴ For hydrogen underpotential deposition, carbon monoxide oxidation, and mercury underpotential deposition, Coulombic charge conversion values were determined from polycrystalline Ir and Ru electrodes, assuming a roughness factor of 1.2. Individual conversion factors for each catalyst were calculated as an average of these values (Ir/Ru), based on their bulk composition in ICP-MS and assumed similar surface/bulk composition.

Additionally, capacitance values were derived from cyclic voltammograms. Voltammograms taken in the potential range 0.025–1.5 V vs RHE at a scan rate of 20 mV s^{-1} in a nitrogen-saturated 0.1 M perchloric acid electrolyte and capacitances were calculated in the range 0.8–1.4 V vs RHE. Capacitances were a function of the specific capacitance of the elements involved, the degree of oxidation, and the catalyst loading (layer thickness). Values were therefore not converted into ECAs but used qualitatively to assess the degree of oxidation.

Catalyst stability was evaluated with RDE half-cells with a 2 V hold for 13.5 h following testing for initial activity and ECA.

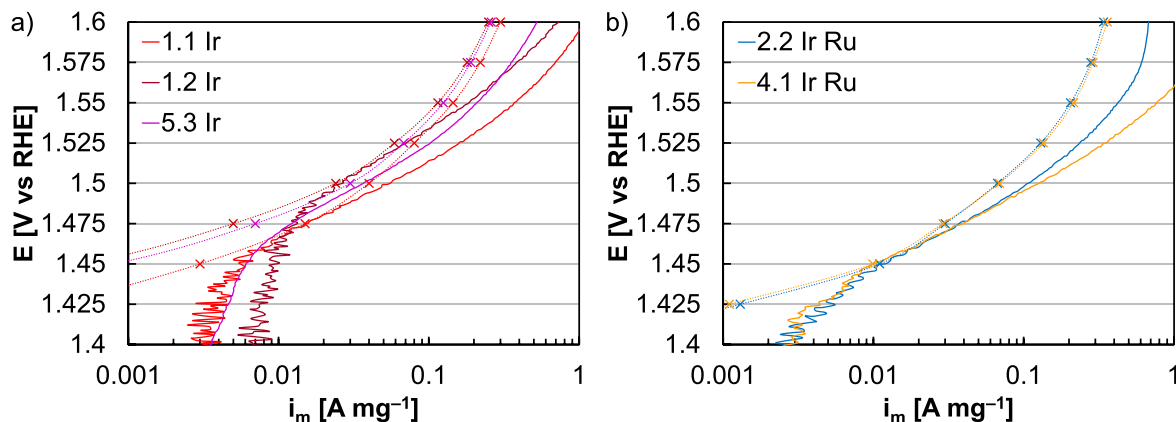


Figure 1. Tafel plots of select (a) Ir-only and (b) Ru- and Nb-containing catalysts, with data taken during linear sweep voltammograms (solid line) and successive chronoamperometry tests (\times with dotted line).

Following the potential hold, aliquots of the electrolyte were tested for dissolved catalyst (Ir, Ru, Nb) with ICP-MS. Working electrodes were rinsed with water and dried to normalize the electrodes against one another (reproducibility) and against their initial activity. After the electrodes dried, they were retested for OER activity and ECA in a fresh electrolyte. Durability data in this study was reported following the rinsing/drying step and the raw current during the potential hold was not presented, due to the large transport impact that lowers the current response and was not indicative of a relevant loss mechanism.⁴⁰ This process (rinse/dry) resulted in minimal loss for the Ir oxide baseline and ECA losses for other catalysts that were proportional to increased dissolution rates. This indicated that bubble formation/transport did not increase stability losses, and these results were consistent with past studies.^{8,31,34} Transport, however, is still a concern in RDE stability evaluations and bubble formation limits site-access during testing, lowering OER activity losses and catalyst dissolution rates. Due to experimental setup and electrode geometry, these issues are different in ex- and in-situ testing; catalyst-specific accelerated stress tests in MEAs, however, have similarly observed gas blinding, where loss rates at higher cell potential were less than expected.⁴¹ While linking ex- and in-situ durability testing is complicated, reasonable and qualitative assessments are possible in RDE half-cells, provided that the user is cognizant of relevant baselines (metal/oxide) and that differences in electrode loading, oxide content, and electrolyte (free vs membrane) dramatically impact loss rates.^{34,41}

MEA testing was conducted using Nel's 28 cm² commercial cell stack hardware. For all configurations, Nafion N117 was used and electrodes were fabricated as gas diffusion electrodes (GDEs), using a spray coater. Hydrogen electrodes were made using the same process, with Pt Black from Alfa Aesar. Target loadings for the oxygen and hydrogen electrodes were 2.0 mg cm⁻² each. Operational testing was conducted at 50 °C and hydrogen generation pressure of 30 bar.

Results and Discussion

RDE half-cell screening was completed on 11 novel materials, segregated into rounds (Rounds 2–5) based on when they were received. Segregation into Rounds also served to separate materials based on the synthesis approach and catalyst manufacturer. Ir metal (Johnson Matthey, C2026/160000) and Ir oxide (Alfa Aesar, 43396) catalysts (Round 1) were included as baselines to bracket the developed materials.³¹

Ex-situ testing.—In addition to the elemental composition (Ir, Ru, Nb), the metal/oxide content had a clear impact on ex-situ OER activity and stability. Separating metal/oxide content was also critical to explaining RDE trends and setting realistic expectations

of MEA performance.³⁴ To assess differences between metal/oxide participation in electrochemical measurements, several methods were used to approximate surface areas and included hydrogen underpotential deposition, mercury underpotential deposition, capacitance, and BET. These measurements are based on past efforts that compared different surface area techniques on baseline catalysts (Round 1), and this study did not develop or modify experimental protocols.³² From past studies, catalysts with more metallic surfaces adsorbed protons (hydrogen underpotential deposition) and carbon monoxide, had thinner capacitances, and for the metal baseline (1.1 Ir, Johnson Matthey), produced ECAs from hydrogen underpotential deposition (28.7 m² g_{Ir}⁻¹, Fig. 2a) and carbon monoxide stripping (30.8 m² g_{Ir}⁻¹) that were similar to BET values (34 m² g_{Ir}⁻¹).³² More oxidized surfaces, however, did not participate in hydrogen underpotential deposition or carbon monoxide stripping and had thicker capacitances, irrespective of their surface area (1.2 Ir, Alfa Aesar, 35 m² g_{Ir}⁻¹ with BET, Fig. 2a).³² While catalyst capacitance is not surface sensitive and a function of the specific capacitance of a material and the catalyst layer thickness, capacitance measurements were included since they are useful in qualitatively assessing oxide content through the catalyst bulk. Additionally, mercury underpotential deposition was previously used to determine Ir metal/oxide ECAs and applied to these materials.³² ECAs from this method were used to assess the number of sites available electrochemically, compare the relative contributions of hydrogen underpotential deposition and capacitance, and determine site-specific OER activities.

When comparing these methods, two trends were found. (Figs. 3a, 3b) First, most of the developed catalysts (Rounds 2–5) showed characteristics consistent with a combination of metal and oxide, with some hydrogen underpotential deposition and moderate capacitances (Fig. 2). These findings were supported by mercury underpotential deposition measurements, where hydrogen underpotential deposition did not account for the total ECAs (Fig. 3a). In a couple of cases (4.1 Ir Ru, 4.2 Ir Ru), the ECAs from hydrogen and mercury underpotential deposition were similar, indicating that the catalyst surfaces were primarily metallic. In several other instances, however, small capacitances were found with minimal (3.1 Ir, 3.2 Ir, Fig. 2c) or no (5.3 Ir, Fig. 2e) hydrogen underpotential deposition, indicating that while the surface was not metallic enough to adsorb protons, the catalyst may not have been completely oxidized through the bulk. Second, mercury underpotential deposition ECAs were not always comparable to BET surface areas, particularly for catalysts with surface areas (BET) over 100 m² g⁻¹. This was likely due to poor catalyst utilization at standard loadings (17.8 μg cm⁻²) and may require lower loading to access available surfaces and maximize OER mass activity. Low ECAs may also be impacted by catalyst porosity, either due to difficulties accessing smaller pores with mercury or reducing surfaces to participate in mercury

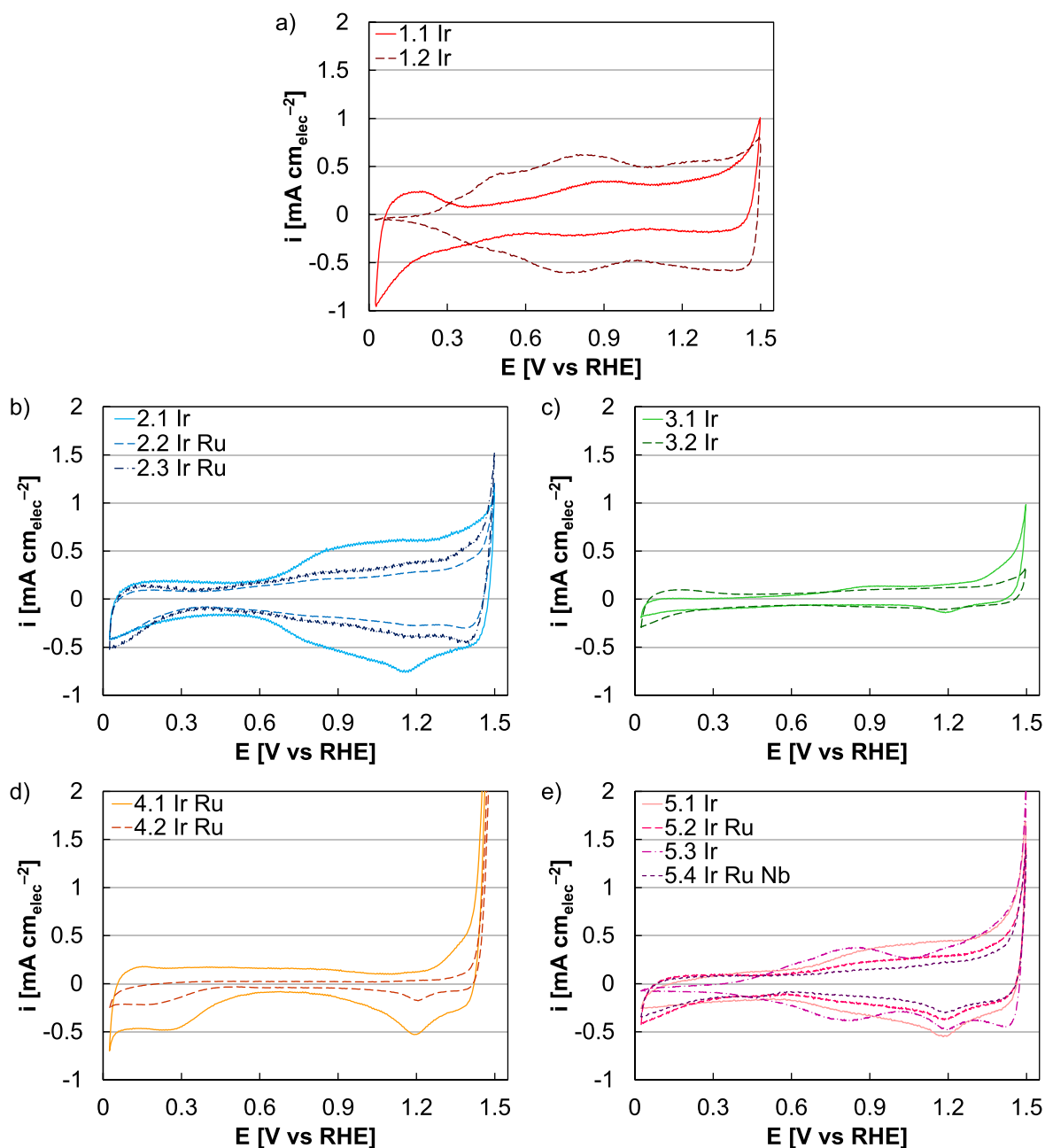


Figure 2. Cyclic voltammograms of examined catalysts in the range 0.025–1.5 V, in a 0.1 M perchloric acid electrolyte. Catalysts were binned based on test round (chronological) and included (a) 1.1 Ir and 1.2 IrO₂ baselines, (b) 2.1 Ir, 2.2 Ir Ru, and 2.3 Ir Ru, (c) 3.1 Ir and 3.2 Ir, (d) 4.1 Ir Ru and 4.2 Ir Ru, and (e) 5.1 Ir, 5.2 Ir Ru, 5.3 Ir, and 5.4 Ir Ru Nb.

underpotential deposition. Differences between capacitance, hydrogen underpotential deposition, and mercury underpotential deposition stress the difficulty of determining catalyst surface area and of assigning metal/oxide surfaces with mixed oxide content. Additionally, BET characterization may also be useful or necessary to monitor the accuracy of ECA measurements.

OER activities in RDE were determined with linear sweep voltammograms and characteristics were consistent for the materials evaluated (Fig. 4). Tafel slopes in the kinetic region ranged from 46.8 to 52.6 mV dec⁻¹ and comparable values may indicate similarities in mechanism (Table I). At higher current density, transport differences were found which may be due to catalyst porosity and the ability to handle bubble formation and detachment. At lower current density, differences in the flattened (vertical) region of the Tafel plots was due to differences in capacitance and followed expected trends from cyclic voltammograms (Fig. 2). At a potential

of 1.525 V, the OER activities were within the kinetic region and compared on a mass and site-specific basis, using mercury underpotential deposition to calculate the specific activity (Figs. 3c, 3d). In general terms and as expected, the specific activities of the Ru- and Nb-containing catalysts tended to be larger than Ir-only catalysts. The exception was the Ir metal baseline (1.1 Ir) which had a high intrinsic activity due to the high metal content, with subsurface metal likely straining the oxide skin at OER-relevant potentials.³⁴ These two factors (composition, oxide content) tended to dictate OER activity of the developed catalysts (Rounds 2–5), where Ru/Nb inclusion and high metal content resulted in higher activity.

For specific catalyst subsets, Round 2 had moderate specific OER activities that were similar to the Ir oxide baseline (Figs. 3c, 3d). The activity was consistent with XRD patterns, which showed oxide reflections, and RDE, where mismatches in hydrogen and mercury underpotential deposition ECAs suggested mixed metal/oxide

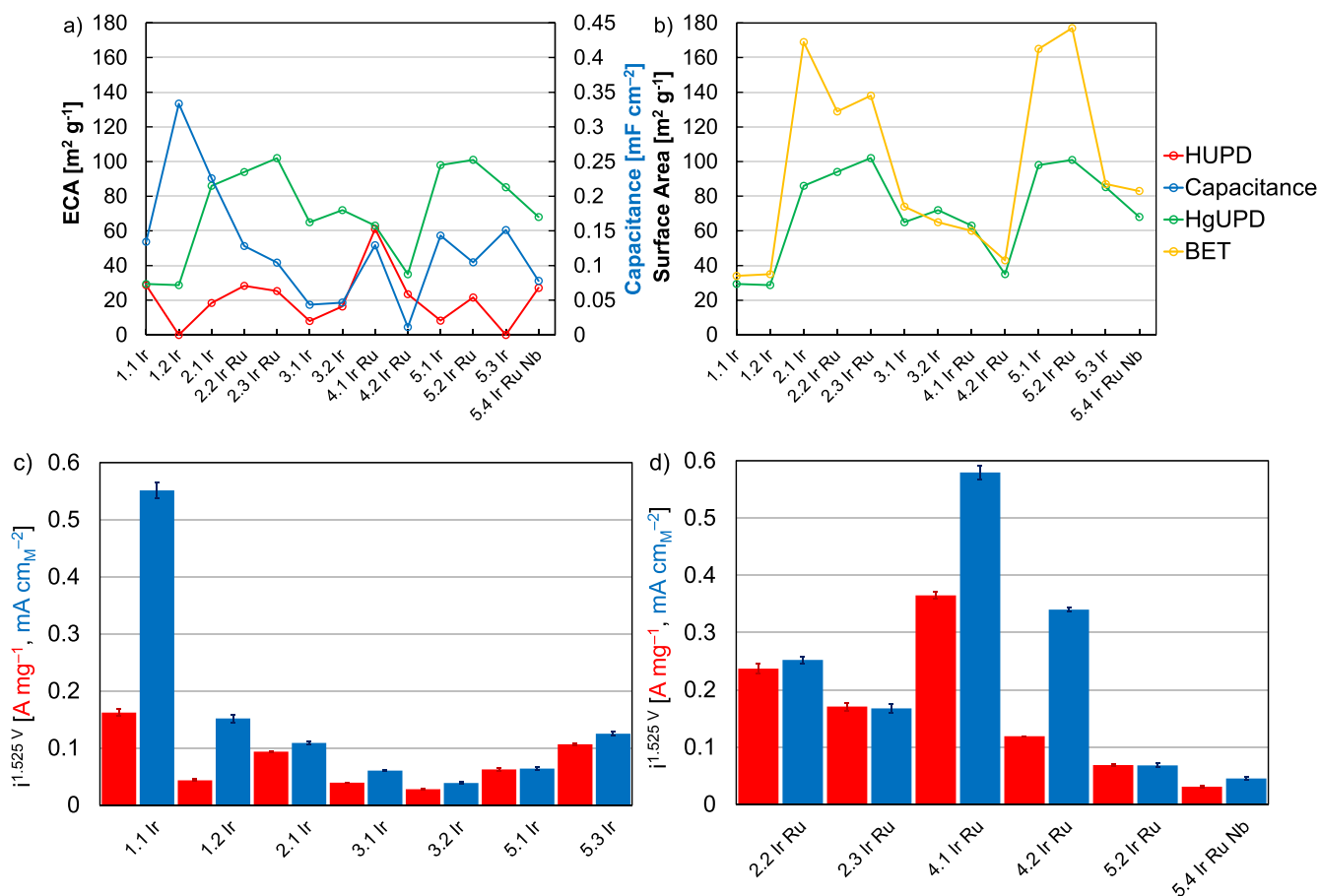


Figure 3. (a) Catalyst ECAs by hydrogen underpotential deposition (red), capacitances (blue), and ECAs by mercury underpotential deposition (green). (b) Catalyst ECAs by mercury underpotential deposition (green) and surface areas by BET (yellow). OER mass (red) and site-specific (blue) activities of (c) Ir-only and (d) Ru- and Nb-containing catalysts.

content near the surface (Figs. 3a, 5a). As expected, the activity of 2.2 Ir Ru and 2.3 Ir Ru was higher (compared to 2.1 Ir) and likely due to the addition of Ru. In Round 3, the specific activities were the lowest of any of the developed catalysts, due to the lack of Ru and the high oxide content. Minimal participation in hydrogen underpotential deposition suggested a primarily oxide surface; the emergence of metal XRD reflections (Ir (111) and (200)), however, confirmed the presence of metal in the catalyst bulk. In Round 4, higher specific activity was consistent with high Ru content. Higher activity than other Ru-containing catalysts (Round 2, 5) was likely due to the high amount of metal, evident from similarities in hydrogen/mercury underpotential (surface composition) and XRD patterns (bulk composition). Since the Ir/Ru composition of these two catalysts was similar, differences in activity may have been impacted by the metal/oxide composition, where 4.2 Ir Ru had smaller specific activity and appeared to have more oxides at the surface (slight gap between hydrogen/mercury underpotential deposition). In Round 5, the specific activities were moderate and similar to other catalysts that were heavily oxidized. High degrees of oxidation were consistent with XRD patterns and electrochemical results, where differences between the hydrogen and mercury participation suggested a heavily oxidized surface. For 5.2 Ir Ru and 5.4 Ir Ru Nb, a significant activity benefit was not found and may be due to the small Ru content. Although the higher metal content (modest hydrogen underpotential deposition) may have adversely impacted activity due to Ru/Nb dissolution during conditioning, evidence of dissolution due to conditioning was not found in ICP-MS. Of the materials evaluated, 4.1 Ir Ru had the highest mass OER activity (0.37 A mg⁻¹ at 1.525 V), 8.4 times greater than

the Ir oxide baseline due to a combination of higher surface area (2.2 times) and specific activity (3.8 times).

The electrochemical and structural properties of the examined catalysts were evaluated for trends, focusing on the impact on site-specific activity (site quality). Materials were separated based on composition (Ru- or Nb- inclusion red, Ir-only blue); specific designations were made for the Ir baselines (open blue squares) and catalysts containing a small amount of Ru (open red circles), since their activities were similar to the Ir-only catalysts. Generally, either Ru-inclusion or a high metal content were needed for higher RDE activity, expected and consistent with past findings in literature (Fig. 6a).^{10,11,34} Although composition (elemental, metal/oxide) was clearly a principal factor, bulk crystallinity may also affect OER activity, with more amorphous surfaces improving activity through defects/distortions weakening O-binding.^{42,43} While no consistent trend was found for the materials overall, lower crystallite size correlated to higher performance within the individual material sets evaluated (Fig. 6b). The trend held when focusing on mixed oxides (Rounds 2–5) and separating materials into those that were Ir-only or contained Ru/Nb. This required grouping low Ru content catalysts with the Ir-only; the Ir metal baseline (1.1 Ir) was also a clear outlier. While a loose relationship between crystallinity and activity was found, distortions and reordering at electrolysis-relevant potentials may amorphize Ir surfaces and negate the impact of bulk material properties ex-situ.³⁴ Additionally and when comparing activities to catalyst ECAs (mercury underpotential deposition), no clear relationship between ECA and specific activity (particle size effect) was found (Fig. 6c). A clear trend was also not found between activity and

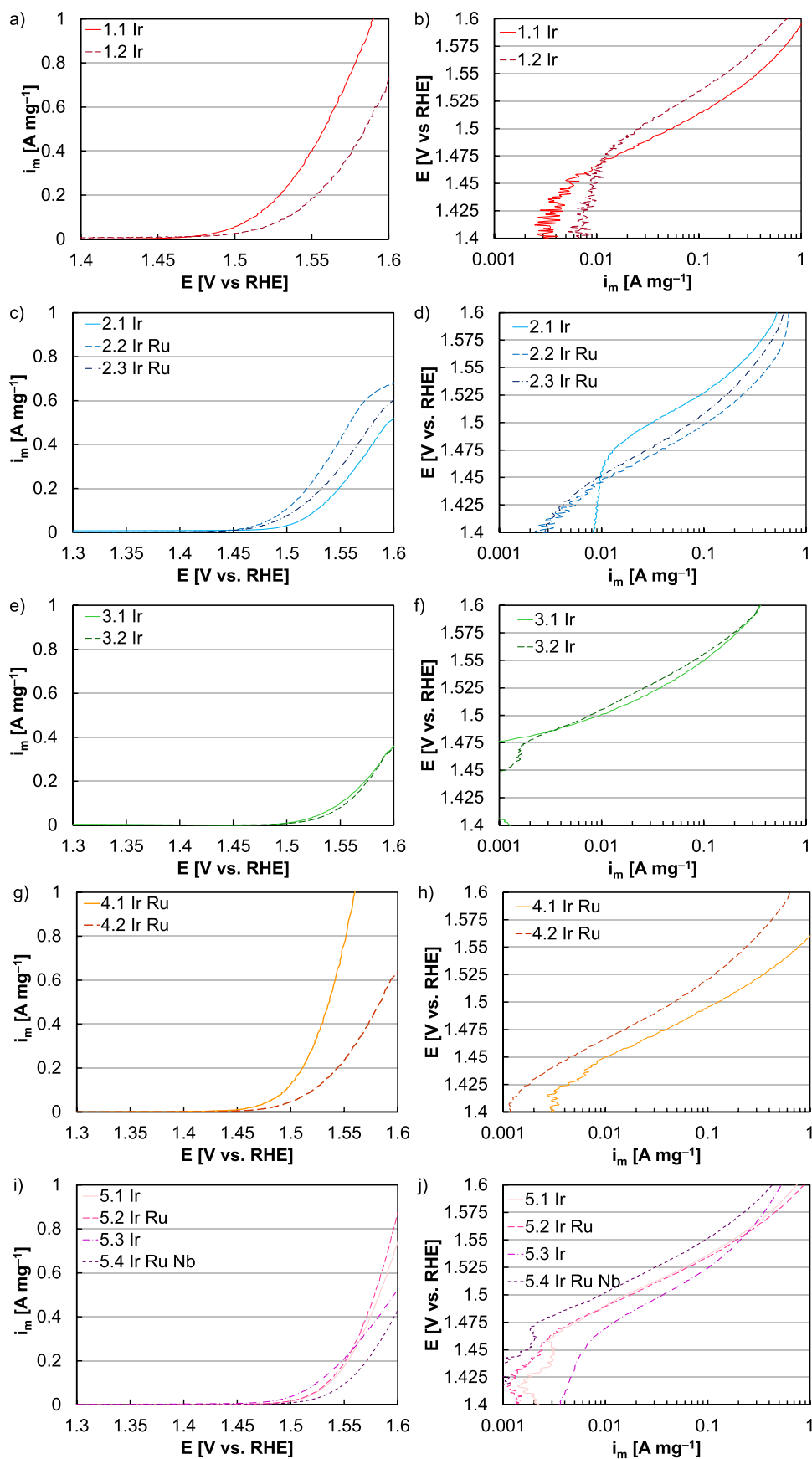


Figure 4. OER linear sweep voltammograms of examined catalysts in a 0.1 M perchloric acid electrolyte, at a scan rate of 20 mV s^{-1} and a rotation speed of 2500 rpm. Catalysts were binned based on test round (chronological) and included (a–b) 1.1 Ir and 1.2 Ir, (c–d) 2.1 Ir, 2.2 Ir Ru, and 2.3 Ir Ru, (e–f) 3.1 Ir and 3.2 Ir, (g–h) 4.1 Ir Ru and 4.2 Ir Ru, and (i–j) 5.1 Ir, 5.2 Ir Ru, 5.3 Ir, and 5.4 Ir Ru Nb. Subfigure (a–b) was adapted from.³¹

catalyst morphology in microscopy (Figs. 3c, 3d, 5b–5e). Catalyst differences were found, and the materials contained a wide range of aggregate sizes with qualitative differences in surface

roughness. No consistent correlation, however, was observed and small aggregate size accounted for both the high (Round 4) and low (Round 3) performers in RDE OER.

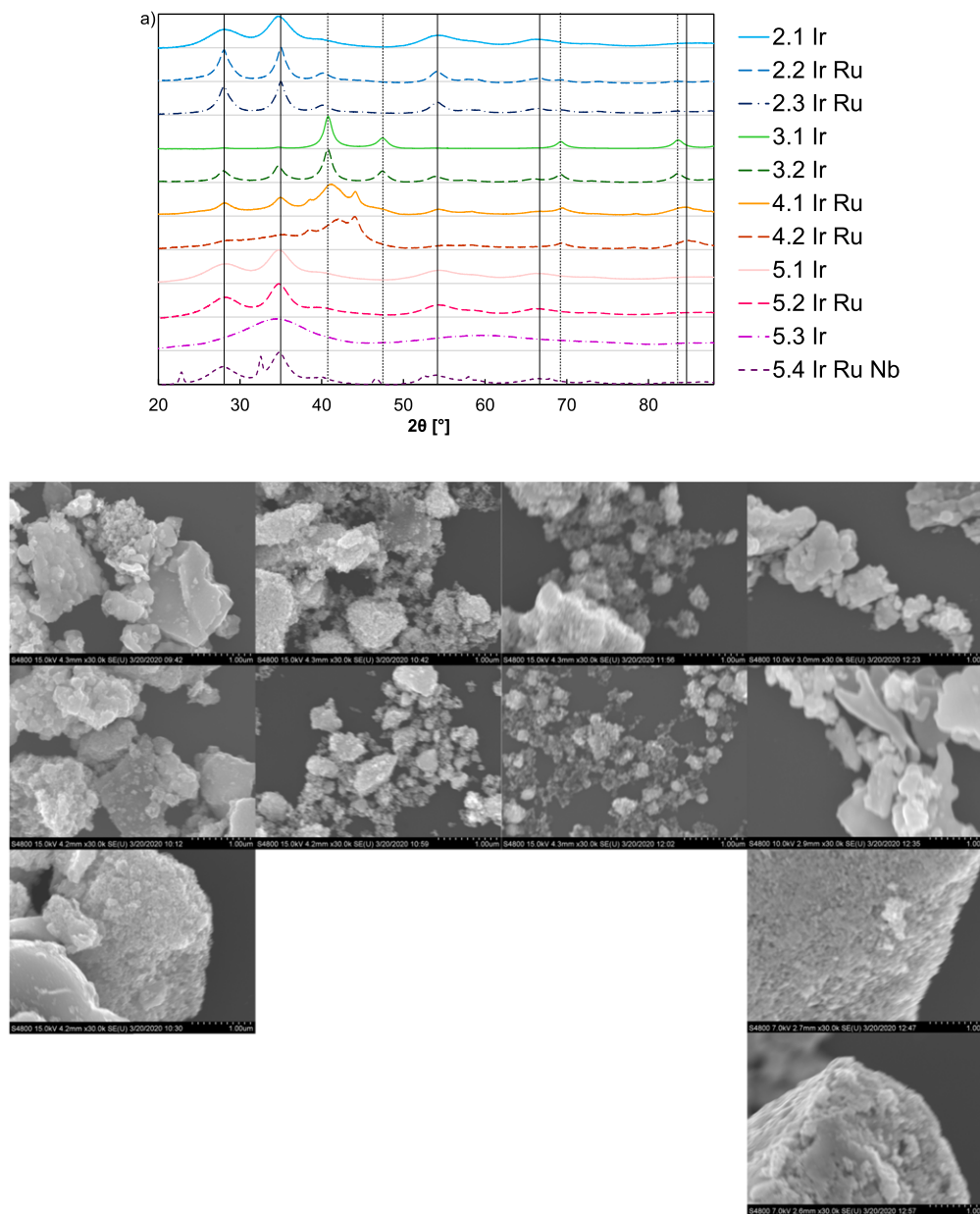


Figure 5. (a) XRD patterns of developed catalysts, Rounds 2–5. SEM images of (b) Round 2 (2.1 Ir, 2.2 Ir Ru, 2.3 Ir Ru), (c) Round 3 (3.1 Ir, 3.2 Ir), (d) Round 4 (4.1 Ir Ru, 4.2 Ir Ru), and (e) Round 5 (5.1 Ir, 5.2 Ir Ru, 5.3 Ir, 5.4 Ir Ru Nb) catalysts.

RDE durability testing was completed with a 2 V potential hold for 13.5 h, previously used to determine catalyst dissolution rates in OER and correlated to MEA durability losses at low loading and intermittent operation (Figs. 7a–7d).⁴¹ From the Ir metal (1.1 Ir) and oxide (1.2 Ir) baselines, two extremes were found. Stability testing of Ir metal resulted in large amounts of dissolution (80%) and complete activity loss; for Ir oxide, however, little dissolution (6%) or activity change (8% mass activity decrease) were found, consistent with past studies.^{31,34} Of the developed catalysts (Rounds 2–5), a range of dissolution rates and durabilities were observed (Fig. 7e). Generally, the OER activity losses tended to be larger for catalysts that included Ru and Nb, expected due to the higher dissolution rates and increased favorability of dissolved species at elevated potential.^{10,11} Activity losses also tended to be larger for catalysts that were more metallic (surface/bulk), due to the higher dissolution rate and increased dissolution kinetics of metals compared to oxides.³⁴

Of the developed catalysts (Round 2–5), durability losses in Round 4 were the most severe and were likely affected by the high

Ru composition and metal content (Figs. 7a, 7d). Within other Ru/Nb containing catalysts, Round 2 losses were moderate. While the high Ru content clearly increased activity losses compared to 2.1 Ir, the higher oxide content likely lessened losses compared to Round 4. Similarly for Round 5 catalysts (5.2 Ir Ru, 5.4 Ir Ru Nb), the durability losses were small due to a combination of lower Ru/Nb content and lower metal content. Of the developed catalysts, 2.2 Ir Ru had the largest OER activity (0.18 A mg^{-1} at 1.525 V) following RDE durability testing. Compared to the Ir oxide baseline (1.2 Ir), the post durability activity of 2.2 Ir Ru was 4.4 times greater, primarily due to higher specific activity (2.9 times, 47% greater ECA).

For the developed Ir-only catalysts, the activity losses during a 2 V potential hold were small and expected due to the lack of Ru/Nb (Figs. 7a, 7c). Compared to the metal/oxide baselines, the activity losses were slightly larger than 1.2 Ir (oxide) and much smaller than 1.1 Ir (metal); these results were expected since relatively small metal composition was found during ECA measurements and primarily oxide reflections were found in XRD. Two specific

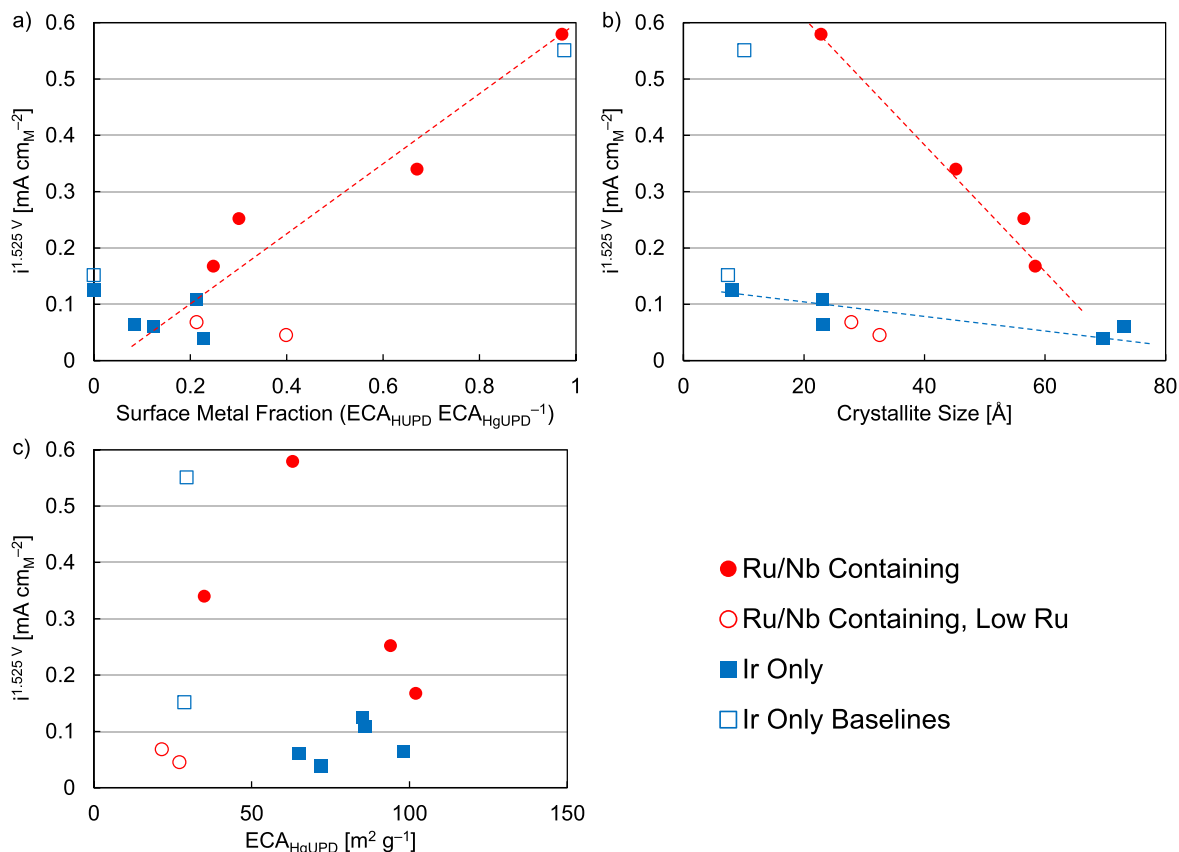


Figure 6. Catalyst site-specific activity as a function of the (a) surface metal content, or the ratio of the metal ECA (hydrogen underpotential deposition) to the total ECA (mercury underpotential deposition), (b) crystallite size, and (c) total surface area (mercury underpotential deposition). Catalysts were separated into those containing Ru/Nb, including moderate (red solid circles) and low (red open circles) Ru content, and those that were Ir-only, including developed (blue solid squares) and baseline (blue open squares) materials. General trendlines (dashed red, blue) were included in subfigures (a) and (b) to aid visually.

instances of interest were found. In the first, very small activity losses and dissolution were observed on 3.1 Ir and 3.2 Ir, although both showed Ir metal in XRD patterns. This may indicate that oxidized surfaces can delay or minimize metal core dissolution and activity loss. In the second, relatively large losses were found for 5.3 Ir even though no metal reflections (XRD) or participation in hydrogen underpotential deposition were found. It was possible that subsurface metal (less crystalline, not detected in XRD) and a thin oxide skin resulted in higher loss. Aside from oxide content, however, other material properties (crystallinity, structure) may have contributed.

In-situ testing.—MEA testing was conducted using Nel's 28 cm² commercial cell stack hardware. For all configurations, Nafion N117 was used and electrodes were fabricated as gas diffusion electrodes (GDEs), using a spray coater. Hydrogen electrodes were made using the same process, with Pt Black from Alfa Aesar. Target loadings for the oxygen and hydrogen electrodes were 2.0 mg cm⁻² each. Operational testing was conducted at 50 °C and hydrogen generation pressure of 30 bar.

MEA performance testing was used to assess RDE evaluations as a predictive tool in OER for low temperature electrolysis. Comparisons between ex- and in-situ measurements are inherently complicated for several reasons. While MEAs have relatively large ohmic loss (depending on membrane thickness), RDEs are typically ohmic-corrected, can accentuate kinetic differences, and have larger transport limitations. Catalyst layer requirements (loading, ionomer content, porosity) in RDEs/MEAs are also different, and different degrees of optimization can result in the reordering of catalyst performances.⁴⁴ Furthermore, past efforts have shown that RDE can overestimate the activity and underestimate the durability of more

metallic catalysts due to differences in the temperature, time, and potential requirements between the two approaches.³⁴ In spite of these difficulties, RDE was previously found to be a reasonable predictor of MEA kinetics with limited materials sets (Ir-only).³⁴ Comparing RDE/MEA results in this study was seen as a more rigorous test of RDE due to the inclusion of elements beyond Ir (Ru/Nb) and mixed metals/oxides.

Within individual material sets, consistency was generally found between RDE activity and MEA kinetics. In Round 2, trends in OER mass activities (RDE) matched MEAs (2.1 Ir < 2.3 Ir Ru < 2.2 Ir Ru), where the activity of 2.1 Ir was likely lower due to the lack of Ru (Fig. 8b). In Rounds 3 and 4, OER mass activities (RDE) followed the trend 3.2 Ir < 4.2 Ir Ru < 4.1 Ir Ru. In MEAs, the 3.2 Ir performance was similarly the lowest within the material set (likely due to the lack of Ru) and of all catalysts evaluated. The performances of 4.1 Ir Ru and 4.2 Ir Ru, however, were similar (Fig. 8c). Compositional differences between these catalysts were relatively small in terms of Ru (4.1 Ir Ru, 30.4% Ru; 4.2 Ir Ru, 42.1% Ru) and oxide (4.1 Ir Ru, 10.6% Ru; 4.2 Ir Ru, 3.6% Ru) content. These differences further did not impact RDE/MEA comparisons in expected ways, where higher Ru (dissolution during conditioning) or oxide content (growth during conditioning) did not result in lower MEA performance. 4.1 Ir Ru, however, did have a higher ECA (63 m² g⁻¹) than 4.2 Ir Ru (35 m² g⁻¹) which may not directly translate to MEAs due to differences in catalyst loading and electrode structure (site utilization). In Round 5, RDE found the activity trend 5.4 Ir Ru Nb < 5.1 Ir, 5.2 Ir Ru < 5.3 Ir. These trends matched MEA performances, where 5.1 Ir and 5.2 Ir Ru were similar and bracketed by 5.4 Ir Ru Nb (low performance) and 5.3 Ir (high performance) (Fig. 8d). In this sense and within specific material sets, RDE appeared to a reasonable predictor of MEA kinetic trends

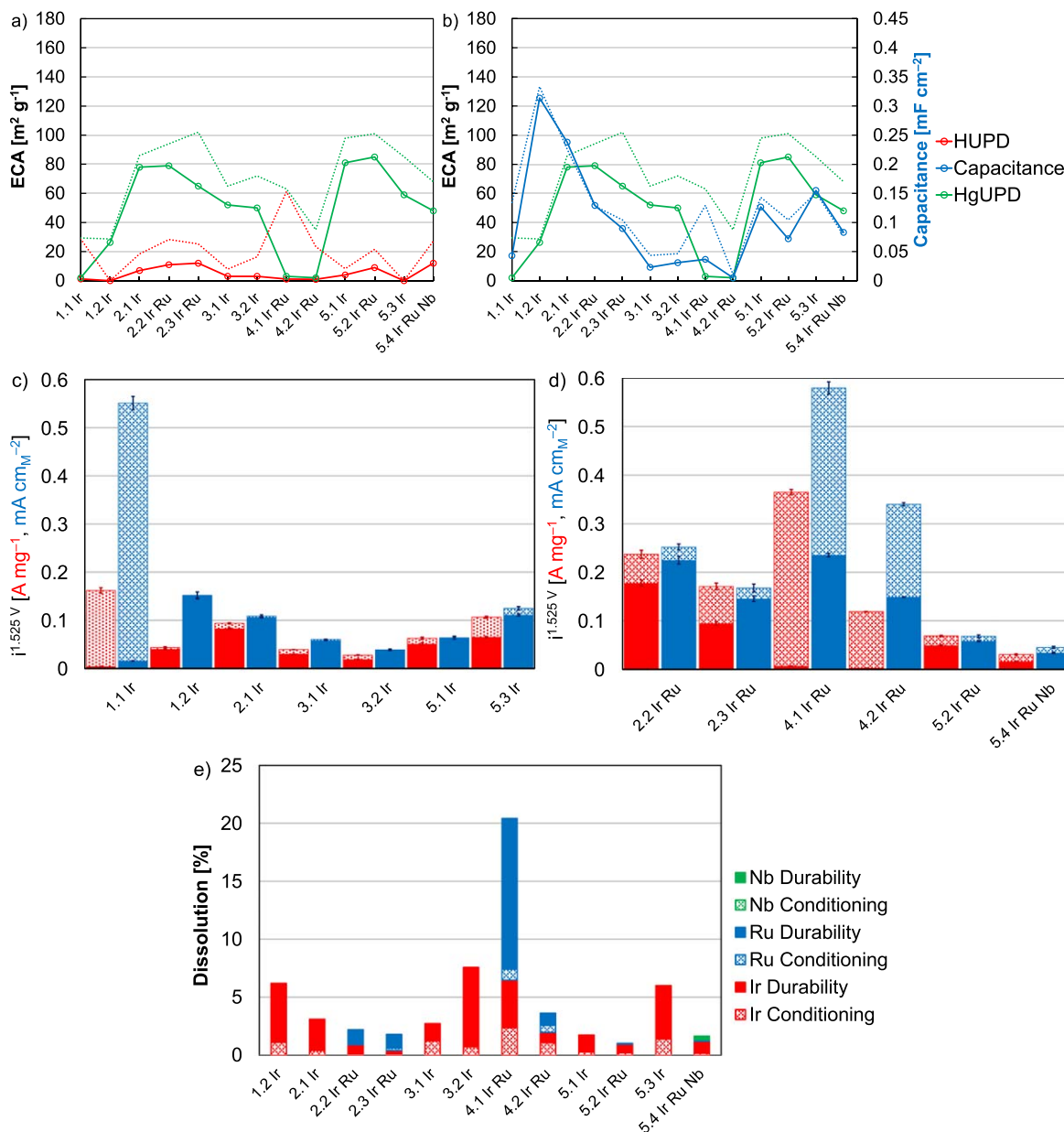


Figure 7. (a) Catalyst ECAs by hydrogen underpotential deposition (red) and mercury underpotential deposition (green), prior to (dotted line) and following (solid line) durability testing. (b) Catalyst capacitances (blue) and ECAs by mercury underpotential deposition (green), prior to (dotted line) and following (solid line) durability testing. OER mass (red) and site-specific (blue) activities of (c) Ir-only and (d) Ru- and Nb-containing catalysts. (e) Catalyst dissolution during conditioning and durability testing, with Ir (red), Ru (blue), and Nb (green) quantified.

that included Ru/Nb additions and differences in elemental composition.

When comparing all evaluated catalysts, however, differences were found between ex- and in-situ results in several instances. As expected, RDE testing likely overestimated the kinetic performance of metals and more metallic catalysts due to the lower temperature and less time spent at elevated potential.³⁴ This was the clearest for 4.1 Ir Ru and 4.2 Ir Ru, which were primarily metals (similar ECAs from hydrogen and mercury underpotential deposition) that produced high ex-situ activity and some of the lowest in-situ kinetics. For the other catalysts, most had characteristics consistent with mixed metals/oxides and the activity discrepancies were smaller. Many saw activity advantages in RDE compared to the oxide baseline (1.2 Ir) that weakened in MEAs, and included instances

where the MEA kinetics dropped to a level similar to (2.3 Ir) and less than (2.1 Ir) the baseline catalyst. These differences stress the need to either account for metal/oxide composition or to use multiple baselines (metal, oxide) in RDE to set more realistic expectations of MEA performance.

In durability, the trends found in RDE are expected and include higher dissolution and activity loss rates for catalysts containing other elements (Ru/Nb) and a higher proportion of metals. These trends are generally expected from past MEA results at low catalyst loading (shorter duration) and a smaller subset of these materials at higher loading (longer duration).^{34,35,38} Work is currently underway to screen a broader set of these catalysts for MEA durability, and to ensure that test conditions (catalyst loading, duration) are representative of long-term operation and device lifetime. While these trends

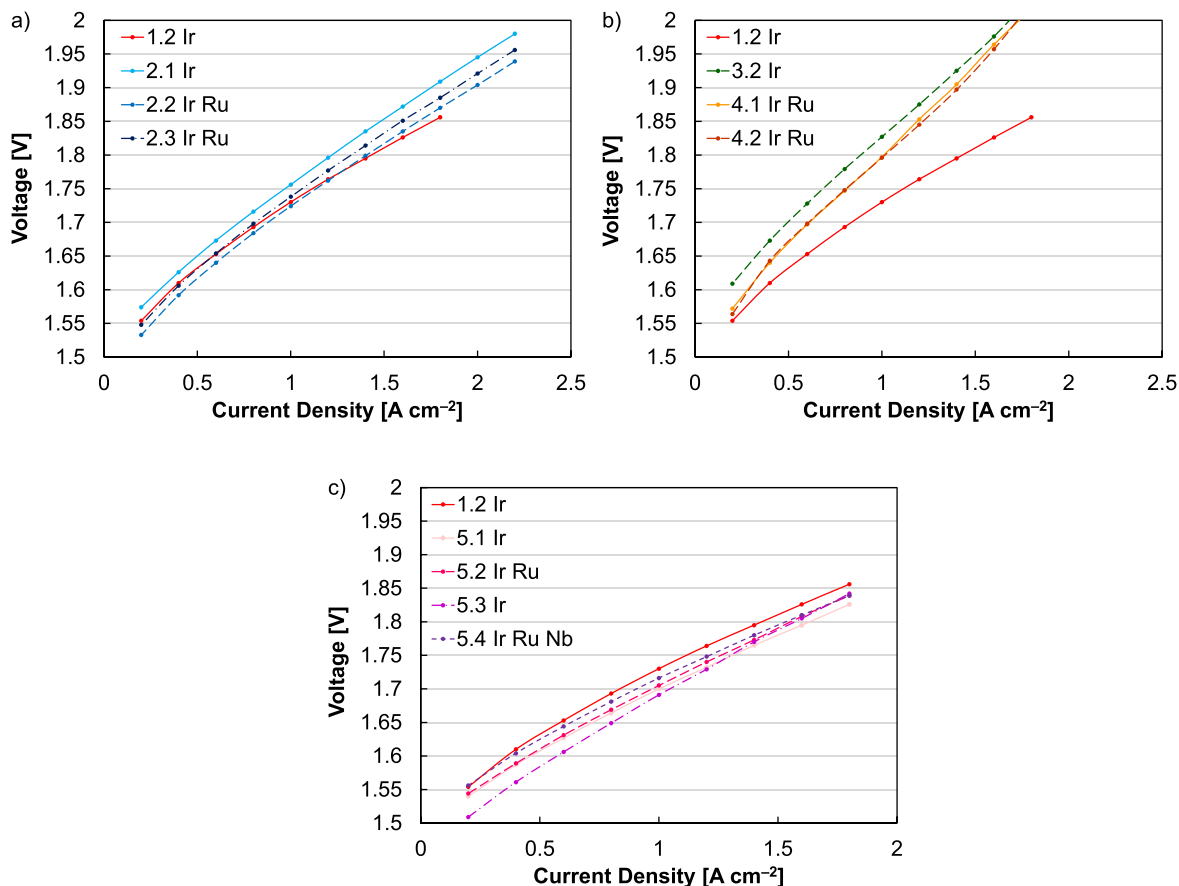


Figure 8. MEA performances of examined catalysts, including (a) 2.1 Ir, 2.2 Ir Ru, and 2.3 Ir Ru, (b) 3.2 Ir, 4.1 Ir Ru, and 4.2 Ir Ru, and (c) 5.1 Ir, 5.2 Ir Ru, 5.3 Ir, and 5.4 Ir Ru Nb. Catalyst performances were binned based on test round (chronological) and included the 1.2 Ir oxide baseline.

are expected to hold, it is also likely, however, that high RDE loss rates (Ru/metal in particular) overestimate performance decreases in MEAs and are primarily useful as a qualitative comparison.³⁴

Conclusions

In this study, Ir-based oxygen evolution catalysts were screened for activity with RDE half-cells. The samples evaluated included Ir-only nanomaterials and those containing Ru/Nb, and were a combination of metals, oxides, and mixtures. In general, the activities were higher for catalysts that contained Ru and larger amounts of metals; durability, however, was improved for catalysts that were Ir-only and oxides. Although Ru inclusion and metals were necessary for higher ex-situ activity, smaller crystallite sizes within material sets also appeared to improve performance. No correlation, however, was found between surface area (particle size effect) or morphological features and activity.

The performance of these catalysts was also evaluated in MEAs to assess RDE as a predictive tool. In particular, the inclusion of Ru/Nb and mixed metals/oxides allowed for a more robust evaluation than previous efforts. Within individual material sets, RDE was reasonably able to predict the ordering of MEA kinetics, including between catalysts that were Ir-only and those containing Ru/Nb. In the broader sense, however, ex-situ testing did struggle to account for differences in metal/oxide composition, likely due to the lower potential, lower temperature, and shorter time in which testing took place. This issue clearly appeared in two ways, where: Round 4 catalysts (primarily metallic) were the highest performing in RDEs but of the lowest performing in MEAs; and most activity advantages compared to the oxide baseline in RDEs weakened in MEAs. These findings stress the need to account for the degree of oxidation, through either multiple baselines (metal/oxide) or surface area evaluation methods

(capacitance, hydrogen/mercury underpotential deposition), to set realistic expectations for device-level performance.

Electrolyzers currently use high catalyst loading since the feed-stock is the primary cost driver and to avoid performance losses associated with thin catalyst layers. As electrolysis shifts to load following low-cost electricity inputs, catalyst development is needed better understand the extent that loading reductions are possible to minimize component cost and how higher performing materials can lessen load requirements. While RDE screening is beneficial for high throughput screening and to avoid the complications of MEA integration, considerations for the oxide content are needed to ensure the approach is reasonably predictive.

Acknowledgments

This work was authored by the National Renewable Energy Laboratory, operated by Alliance for Sustainable Energy, LLC, for the U.S. Department of Energy (DOE) under Contract No. DE-AC36-08GO28308. Funding provided by U.S. Department of Energy Office of Energy Efficiency and Renewable Energy, Hydrogen and Fuel Cell Technologies Office. The views expressed in the article do not necessarily represent the views of the DOE or the U.S. Government. The U.S. Government retains and the publisher, by accepting the article for publication, acknowledges that the U.S. Government retains a nonexclusive, paid-up, irrevocable, worldwide license to publish or reproduce the published form of this work, or allow others to do so, for U.S. Government purposes.

ORCID

Shaun M. Alia <https://orcid.org/0000-0002-7647-9383>
 Grace C. Anderson <https://orcid.org/0000-0002-2723-5024>
 Katherine E. Hurst <https://orcid.org/0000-0003-4596-9504>

References

- B. Pivovar, *H2 at Scale, NREL Workshop* (U. S. Department of Energy Editor) (2016), (https://energy.gov/sites/prod/files/2016/12/f34/fcto_h2atscale_workshop_pivovar_2.pdf).
- B. Pivovar, N. Rustagi, and S. Satyapal, *The Electrochemical Society Interface*, **27**, 47 (2018).
- DOE H2A Production Analysis, *U.S. Department of Energy Office of Energy Efficiency and Renewable Energy* (2018), (<https://hydrogen.energy.gov/h2a-delivery.html>).
- U. Babic, M. Suermann, F. N. Büchi, L. Gubler, and T. J. Schmidt, *J. Electrochem. Soc.*, **164**, F387 (2017).
- K. Ayers, N. Danilovic, R. Ouimet, M. Carmo, and B. Pivovar, *Annual Review of Chemical and Biomolecular Engineering*, **10**, 219 (2019).
- K. Ayers, *Current Opinion in Electrochemistry*, **18**, 9 (2019).
- S. M. Alia, *Current Opinion in Chemical Engineering*, **33**, 100703 (2021).
- S. M. Alia, B. Rasimick, C. Ngo, K. Neyerlin, S. S. Kocha, S. Pylypenko, H. Xu, and B. S. Pivovar, *J. Electrochem. Soc.*, **163**, F3105 (2016).
- K. C. Neyerlin, W. Gu, J. Jorne, and H. A. Gasteiger, *J. Electrochem. Soc.*, **154**, B631 (2007).
- M. Pourbaix, *Atlas of Electrochemical Equilibria in Aqueous Solutions* (National Association of Corrosion Engineers, Houston, Texas) (1974).
- N. Danilovic, R. Subbaraman, K.-C. Chang, S. H. Chang, Y. J. Kang, J. Snyder, A. P. Paulikas, D. Strmcnik, Y.-T. Kim, and D. Myers, *The Journal of Physical Chemistry Letters*, **5**, 2474 (2014).
- T. Reier, M. Oezaslan, and P. Strasser, *ACS Catal.*, **2**, 1765 (2012).
- R. Kötz and S. Stucki, *Electrochim. Acta*, **31**, 1311 (1986).
- M. H. Miles, E. A. Klaus, B. P. Gunn, J. R. Locker, W. E. Serafin, and S. Srinivasan, *Electrochim. Acta*, **23**, 521 (1978).
- R. Forgie, G. Bugosh, K. C. Neyerlin, Z. Liu, and P. Strasser, *Electrochem. Solid-State Lett.*, **13**, B36 (2010).
- I. C. Man, H.-Y. Su, F. Calle-Vallejo, H. A. Hansen, J. I. Martínez, N. G. Inoglu, J. Kitchin, T. F. Jaramillo, J. K. Nørskov, and J. Rossmeisl, *Chem.Cat.Chem.*, **3**, 1159 (2011).
- A. Zlotorowicz, F. Seland, and S. Sunde, *ECS Trans.*, **50**, 71 (2013).
- W. Hu, S. Chen, and Q. Xia, *Int. J. Hydrogen Energy*, **39**, 6967 (2014).
- C. Hao, H. Lv, C. Mi, Y. Song, and J. Ma, *ACS Sustainable Chemistry & Engineering*, **4**, 746 (2016).
- C. Wang, R. B. Moghaddam, and S. H. Bergens, *The Journal of Physical Chemistry C*, **121**, 5480 (2017).
- R. B. Moghaddam, C. Wang, J. B. Sorge, M. J. Brett, and S. H. Bergens, *Electrochem. Commun.*, **60**, 109 (2015).
- T. Reier, Z. Pawolek, S. Cherevko, M. Bruns, T. Jones, D. Teschner, S. R. Selve, A. Bergmann, H. N. Nong, and R. Schlögl, *JACS*, **137**, 13031 (2015).
- H. N. Nong, L. Gan, E. Willinger, D. Teschner, and P. Strasser, *Chem. Sci.*, **5**, 2955 (2014).
- H. N. Nong, H. S. Oh, T. Reier, E. Willinger, M. G. Willinger, V. Petkov, D. Teschner, and P. Strasser, *Angew. Chem. Int. Ed.*, **54**, 2975 (2015).
- W. Sun, Y. Song, X.-Q. Gong, L.-M. Cao, and J. Yang, *Chem. Sci.*, **6**, 4993 (2015).
- V. Pfeifer, T. E. Jones, J. J. V. Vélez, R. Arrigo, S. Piccinin, M. Hävecker, A. Knop-Gericke, and R. J. C. S. Schlögl, *Chem. Sci.*, **8**, 2143 (2017).
- T. Li, O. Kasian, S. Cherevko, S. Zhang, S. Geiger, C. Scheu, P. Felfel, D. Raabe, B. Gault, and K. J. J. Mayrhofer, *Nat. Catal.*, **1**, 300 (2018).
- F. Godínez-Salomón, L. Albitar, S. M. Alia, B. S. Pivovar, L. E. Camacho-Forero, P. B. Balbuena, R. Mendoza-Cruz, M. J. Arellano-Jimenez, and C. P. Rhodes, *ACS Catal.*, **8**, 10498 (2018).
- S. M. Alia, S. Shulda, C. Ngo, S. Pylypenko, and B. S. Pivovar, *ACS Catal.*, **8**, 2111 (2018).
- H. Xu, *High-Performance, Long-Lifetime Catalysts for Proton Exchange Membrane Electrolysis* (2015), (http://hydrogen.energy.gov/pdfs/review15/pd103_xu_2015_o.pdf).
- S. M. Alia and G. C. Anderson, *J. Electrochem. Soc.*, **166**, F282 (2019).
- S. M. Alia, K. E. Hurst, S. S. Kocha, and B. S. Pivovar, *J. Electrochem. Soc.*, **163**, F3051 (2016).
- C. Rakousky, M. Shviro, M. Carmo, and D. Stolten, *Electrochim. Acta*, **302**, 472 (2019).
- S. M. Alia, M.-A. Ha, G. C. Anderson, C. Ngo, S. Pylypenko, and R. E. Larsen, *J. Electrochem. Soc.*, **166**, F1243 (2019).
- S. M. Alia, *H2@Scale: Experimental Characterization of Durability of Advanced Electrolyzer Concepts in Dynamic Loading* (2019), (https://hydrogen.energy.gov/pdfs/review19/ta022_alia_o.pdf).
- A. Weiß, A. Siebel, M. Bernt, T.-H. Shen, V. Tileli, and H. Gasteiger, *J. Electrochem. Soc.*, **166**, F487 (2019).
- S. M. Alia, *H2@Scale: Experimental Characterization of Durability of Advanced Electrolyzer Concepts in Dynamic Loading* (2018), (https://hydrogen.energy.gov/pdfs/review18/tv146_alia_2018_p.pdf).
- K. Ayers, *High Efficiency PEM Water Electrolysis Enabled by Advanced Catalysts, Membranes and Processes* (2020), (https://hydrogen.energy.gov/pdfs/review20/p155_ayers_2020_p.pdf).
- S. P. Kounaves and J. Buffle, *J. Electrochem. Soc.*, **133**, 2495 (1986).
- H. A. El-Sayed, A. Weiß, L. F. Olbrich, G. P. Putro, and H. A. Gasteiger, *J. Electrochem. Soc.*, **166**, F458 (2019).
- S. M. Alia, S. Stariha, and R. L. Borup, *J. Electrochem. Soc.*, **166**, F1164 (2019).
- V. Pfeifer, T. E. Jones, J. J. Velasco Vélez, R. Arrigo, S. Piccinin, M. Hävecker, A. Knop-Gericke, and R. Schlögl, *Chem. Sci.*, **8**, 2143 (2017).
- C. Massué, V. Pfeifer, X. Huang, J. Noack, A. Tarasov, S. Cap, and R. Schlögl, *Chem.Sus.Chem.*, **10**, 1943 (2017).
- S. M. Alia, K. S. Reeves, J. S. Baxter, and D. A. Cullen, *J. Electrochem. Soc.*, **167**, 144512 (2020).